Hindawi
Advances in Materials Science and Engineering
Volume 2021, Article ID 5548004, 9 pages
https://doi.org/10.1155/2021/5548004

*Research Article*

# Effect of the Boron Powder on Surface AISI W2 Steel: Experiments and Modelling

**Marco Antonio Doñu Ruiz**,[1] **David Sánchez Huitron**,[1] **Ernesto David Garcia Bustos**,[2] **Víctor Jorge Cortés Suárez**,[3] **and Noé López Perrusquia**[1]

[1]*Grupo Ciencia e Ingeniería De Materiales, Universidad Politécnica del Valle De México (UPVM), Villa Esmeralda 54910, Estado De México, Mexico*
[2]*Cátedras Conacyt, Universidad De Guadalajara, Guadalajara, Mexico*
[3]*D.F. Área De Ciencia De Los Materiales, Univerisdad Autónoma Metropolitana Unidad Azcapotzalco, Av. San Pablo 180, Azcapotzalco 02200, Mexico*

Correspondence should be addressed to Noé López Perrusquia; noeperrusquia@hotmail.com

Received 10 February 2021; Revised 28 April 2021; Accepted 3 June 2021; Published 15 June 2021

Academic Editor: Hongtao Zhu



The effect of boron powder on surface AISI W2 steel and growth kinetic of the boride layer is studied. Boron powder mixture was used in the powder pack boriding; this process was carried out in the temperature range from 1173 to 1273 K with exposure times ranging from 2 to 8 h. The presence of boride was confirmed by optical microscopy, X-ray diffraction, and the distribution of alloy elements in boride layers with energy-dispersive spectrometry using scanning electron microscopy. A mathematical model of the growth kinetics of the single layer was proposed and boron diffusion coefficient was determined by mass balance equation. The morphology of $Fe_2B$ layer was smooth and boron activation energy in W2 steel was estimated as 187.696 kJ·mol$^{-1}$. The kinetic model was validated with two experimental conditions, a contour diagram describing the evolution of $Fe_2B$ layer as a function of time and temperature parameters for industrial application.

## 1. Introduction

The AISI W2 type tool grade steels are widely used in cutting tools, punches for cold forming, cutting and punching. The boriding thermochemical treatment can improve the mechanical properties and extend the lifetime of the workpieces made of AISI W2 steel. The boriding process is the saturation of boron surface of ferrous and nonferrous alloy in order to increase the hardness and wear resistance in engineering components where industrial applications require properties [1].

In the boronizing process, boron atoms are introduced into the metal lattice at the surface of the workpiece through thermal energy to form borides with the atoms of the substrate. The boriding process applies in the temperature range 1073–1323 K between 0.5 and 10 h and it can be carried out in solid, liquid, or gaseous media and plasma [1, 2]. According to the iron-boron phase diagram [3], two iron borides can be formed, $Fe_2B$ and FeB; the FeB (orthorhombic) phase is more brittle than the $Fe_2B$ (tetragonal) phase.

Powder pack boriding is the most widely favoured boriding technique, due to having relative safety and simplicity. This process can be carried out by three boronizing potential of $B_4C$ powder: low (10% $B_4C$-90% SiC), intermediate (100% $B_4C$), and high (90% $B_4C$-10% $KBF_4$) [4]. In addition, the low and intermediate boronizing potential can form single $Fe_2B$, and the high boronizing potential can form double $Fe_2B$ + FeB phases. The formation of single or double phases depends on the boriding process temperature, the boriding time, the chemical composition of the substrate material, and the boron potential of the boriding medium [5].

The single phase structure ($Fe_2B$) is generally more desirable for the intended application in the industry than the bilayer structure consisting of FeB + $Fe_2B$ because FeB ($2.9\times10^{-8}K^{-1}$) and $Fe_2B$ ($8.7\times10^{-8}K^{-1}$) phases have greatly different coefficients of thermal expansion. Therefore, crack formation is in the region of the FeB/$Fe_2B$ interface of the double layers. The presence of the alloying elements of the substrate influences the morphology of the boride layers, so the smooth shape is obtained in high-alloy steels, whereas in the low alloy steels saw-tooth shape layer is obtained.

The mathematical modeling of the kinetic boriding has gained much attention to simulate the boriding kinetics during these last decades. M. Keddam et al. [6] reported that the modeling of the boriding kinetics is considered as a suitable tool to select the optimum process parameters for obtaining adequate boride layers thicknesses in relation to their practical applications. So, in the literature, there are diffusion models for single phase ($Fe_2B$) [7–10], for two phases (FeB + $Fe_2B$) [11, 12], and for the total layer [13, 14] on different substrates. Some parameters to consider are with or without incubation time, linear or nonlinear profile of boron concentration and boriding process. At the moment, there are no studies on the growth kinetics of $Fe_2B$ layer on the surface of AISI W2 steel.

The purpose of this work was forming boride layers with boron powder mixture with low boronizing potential. A mathematical model of growth kinetic is proposed to estimate the boron diffusion coefficient in $Fe_2B$ layer grown on AISI W2 steel considering the boride time incubation; based on the mass balance equation at the ($Fe_2B$/Fe) interface, the model was used to estimate the boron diffusion coefficient in the temperature range of 1173–1273 K. The estimated boron activation energy was compared with the data available in the literature. The present model was validated by comparing the experimental value of boride layer thickness. Finally, a contour diagram relating the $Fe_2B$ layer thickness with the boriding parameters (temperature and time) was proposed for practical use of this kind of borided steel.

## 2. Mathematical Model of the Growth Kinetics of the $Fe_2B$ Layer

The model considers a diffusion of boron atoms into a saturated iron substrate by forming the $Fe_2B$ layer. The boron concentration profile through the $Fe_2B$ is displayed in Figure 1. $C_{up}^{Fe_2B} = 59.8\,\text{mol m}^{-3}$ and $C_{low}^{Fe_2B} = 59.2\,\text{mol m}^{-3}$ are the same limits in the $Fe_2B$ layer, these values are accepted based on the literature date [9, 15, 16]. In this context, the author Massalski [17] reported that $Fe_2B$ iron borides have a narrow range composition of about 1%.

The Fe phase is present before boriding, and the initial condition of the diffusion problem is given by the following equation [18]:

$$C_{Fe_2B}[(t>0)=0]=0. \tag{1}$$

Also, the boundary conditions (see Figure 1) of the diffusion problem are given by the following equations:

$$\begin{aligned} C_{Fe_2B}\left[x\left[t=t_0^{Fe_2B}(T)\right]=m_0\right] &= C_{low}^{Fe_2B}, \quad \text{for } C_{ads}^{B}<60\times10^{3}\,\text{mol m}^{-3},\\ C_{Fe_2B}[x(t=t_o)=m_0] &= C_{up}^{Fe_2B},\\ C_{Fe_2B}[(t=t_m)=m] &= C_{low}^{Fe_2B},\\ C_{Fe_2B}[x(t=t_m)=m] &= C_0, \end{aligned} \tag{2}$$

where $C_{ads}^{B}$ is the effective adsorbed boron concentration, $m$ is the average thickness of the $Fe_2B$ layer, $t_m$ corresponds to treatment time for the formation of the boride layer with a thickness of $m$, $t$ corresponds to treatment time, $t_0(T)$ is the boride incubation time, and $m_0$ is the thickness of the layer after the nucleation stage [19]. Thus, $m_0 \approx 0$ when compared to the thickness $m$ of the $Fe_2B$ after the boriding process.

With regard to this model, the following assumptions are put forward [10, 16]:

(1) The growth kinetics are controlled by the boron diffusion in the $Fe_2B$ layer

(2) The growth of the boride layer occurs as a consequence of the boron diffusion perpendicular to the specimen surface

(3) Differences in specific volume per solvent atom for $Fe_2B$ phases are accommodated fully in the diffusion direction

(4) The iron boride nucleates after a specific incubation time $t_0(T)$

(5) Planar morphology is assumed for the interface $Fe_2B$/substrate

(6) The effect of alloying elements present on the boron diffusion is neglected

The mass balance equation at the interface $Fe_2B$/Fe [20–22] is described by (3) and shown in Figure 1(a):

$$\begin{aligned} &a_2(A\cdot dm)+\frac{1}{2}a_1(A\cdot dm)\\ &\quad=J_B^{Fe_2B}(x=m)(A\cdot dt_m)\\ &\qquad-J^{Fe}(x=m+dm)(A\cdot dt_m), \end{aligned} \tag{3}$$

where $A$ (=1 × 1) is defined as the unit area, where, from Figure 1(b), $a_1 = C_{up}^{Fe_2B} - C_{low}^{Fe_2B}$ defines the homogeneity range of the phase designed $Fe_2B$, $a_2 = C_{low}^{Fe_2B} - C_0$ is the miscibility gap [15], and $C_0$ is the terminal solubility of the interstitial solute. The concentrations $C_{up}^{Fe_2B}$, $C_{low}^{Fe_2B}$, and $C_0$ are expressed in mol·m$^{-3}$, but $C_0 \approx 0\,\text{mol m}^{-3}$ due to the lower solubility of boron [9, 16].

A linear distribution of the boron concentration with the thickness of the $Fe_2B$ layer is described as follows [11, 23, 24]:

$$C_B^{Fe_2B}[x(t)] = C_{up}^{Fe_2B} + \frac{C_{low}^{Fe_2B} - C_{up}^{Fe_2B}}{m}x(t). \tag{4}$$

The fluxes $J_B^{Fe_2B}$ and $J^{Fe}$ are then given by Flick's first law $J = -D\{dC[x(t)]/dx(t)\}$ as follows:

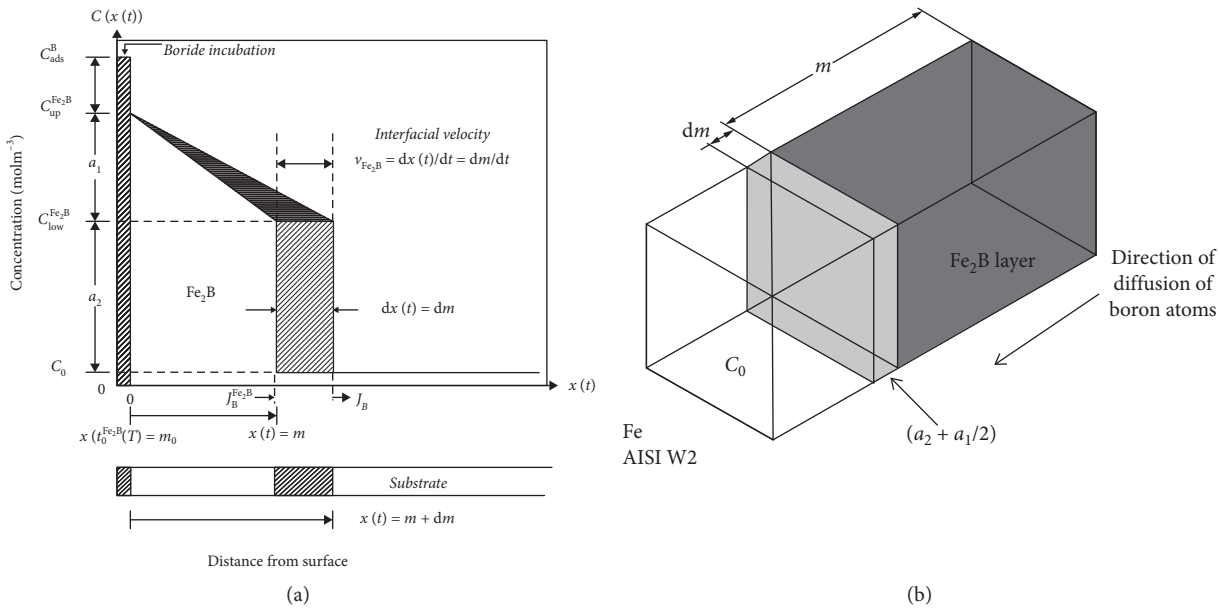


Figure 1: Boron concentration profile: (a) schematic of boron concentration distribution in the $Fe_2B$ and (b) schematic diagram of the mass balance equation at the $Fe_2B$/substrate interface.

$$J_B^{Fe_2B} = D_B^{Fe_2B}\frac{a_1}{m}, \tag{5}$$

where $D_B^{Fe_2B}$ is the diffusion coefficients of boron in $Fe_2B$ layer, $J^{Fe} = 0$ because the boron solubility in the substrate is very low ($C_0 \approx 0\,\text{mol}\,m^{-3}$). By substituting equation (5) into equation (3), the mass balance equation of the interface can be expressed as

$$\left(a_2 + \frac{a_1}{2}\right)\frac{dm}{dt_m} = D_{Fe_2B}\frac{a_1}{m}, \tag{6}$$

$$\frac{dm}{dt_m} = 2D_{Fe_2B}\frac{a_1}{(2a_2 + a_1)m}, \tag{7}$$

The solution to equation (6) can be obtained by considering the parabolic growth equations of the surface layer [11, 21, 22]. The $Fe_2B$ layer growth obeys the power law, of the form

$$m^2 = kt_m = k\left\{t - \left[t_0^{Fe_2B}(T)\right]\right\}, \tag{8}$$

where $m$ indicates average thickness of the $Fe_2B$ layer, $t_m$ corresponds to the treatment time for the formation of the boride layer with a thickness of $m$, $t$ corresponds to treatment time, $t_0^{Fe_2B}(T)$ is the boride incubation time as a function of the boriding temperature, and $k$ is the parabolic growth constant of $Fe_2B$ layers.

Hence, using equation (6), the boron diffusion coefficient at the $Fe_2B$ phase ($D_B^{Fe_2B}$) is determined as

$$D_B^{Fe_2B} = \frac{2C_{up}^{Fe_2B} - C_{low}^{Fe_2B}}{C_{up}^{Fe_2B} - C_{low}^{Fe_2B}}\left(\frac{k}{2}\right)^2. \tag{9}$$

## 3. Experimental

*3.1. The Powder Pack Boriding.* AISI W2 steels with a nominal composition in weight: % C 0.85–1.50, Mn 0.10–0.40, Si 0.10–0.40, Cr 0.15, Ni 0.20, Mo 0.10, W 0.15, and V 0.15–0.35. The samples were sectioned in cubic shape of 500 mm$^3$. Before the boriding, the samples were sanded with silicon carbide abrasive paper up to 600 grit and cleaned with alcohol. The samples were embedded with cylindrical container (AISI 316) having Durborid fresh boron powder mixture inside with an average particle size of 50 $\mu$m as shown in Figure 2. Boron powder mixture contains of $B_4C$ (active source of boron), $Na_3AlF_6$ (activator), SiC (inert filler), and $SiC_8H_{20}O_4$, which is used to protect surfaces; the surface of the sample is covered with a layer of approximately 10 mm thick boron powder mixture with a lid that does not act as a closing device. Boriding was accomplished by placing the container in an electrical resistance furnace model Millennium 2500 from Mexico without the use of inert gases at temperatures of 1173, 1223, and 1273 K with four exposure times of 2, 4, 6, and 8 h for each temperature. After the boriding treatment, the container was removed from the furnace and slowly cooled to room temperature.

*3.2. Experimental Techniques.* The samples were sectioned by diamond saw and resin embedded, polished using standard metallographic techniques, and then etched with Vilella's reagent to reveal their cross-sectional microstructure. The microstructure, morphology, and thickness of boride layers were observed in clear-field through optical microscopy with the aid of a CARL ZEISS AXI0 equipment

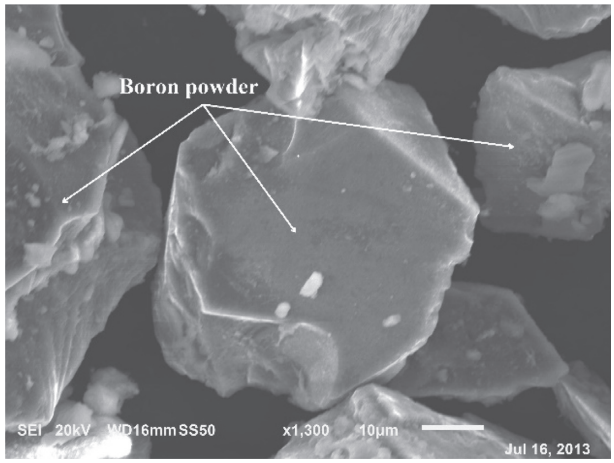


Figure 2: SEM image of particles boron powder mixture.

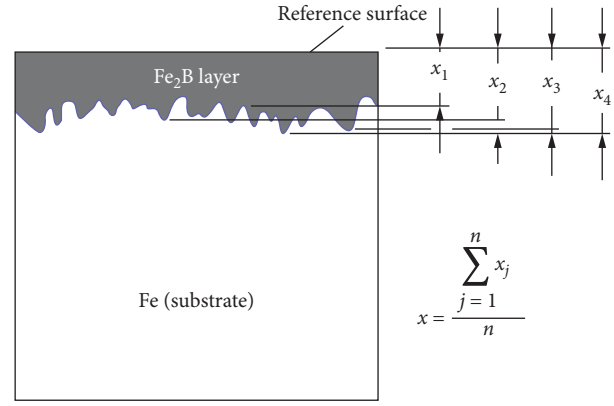


Figure 3: The procedure for estimation of $Fe_2B$ layers thickness in AISI W2 steel.

ZEISS Axio Vert.A1. Moreover, Figure 3 represents a cross section schematic for estimating the thickness of the boride layer [9]. In each sample, fifty measurements were made on different sections of the AISI W2 steel borided; the layer thickness is defined as the average value of along boride teeth [10].

Phases on the boride layers at a temperature of 1273 K with 8 h of exposure were identified by X-ray diffraction (XRD) technique using D8 FOCUS equipment by 35 kV and 25 mA with Cuk$\alpha$ radiation at $\lambda = 1.54$ Å. The diffraction test was undertaken by scanning in the $2\theta$ range from 20° to 100°. The element distributions along a cross section of the boride layer were examined using energy-dispersive spectrometry (EDS) using scanning electron microscope (SEM) JSM-6010-LA JEOL.

## 4. Results and Discussion

*4.1. Boron Powder Mixture (Boriding Process).* The microstructures of the cross-sectional of AISI W2 borided steel with the condition at 1173 K for 2, 4, 6, and 8 h are shown in Figure 4. According to the chemical etching in the cross section of the specimen, clear zones are observed in the image obtained by optical microscopy (OM). These zones have boride layer with $Fe_2B$ and substrate with carbides. In Figure 4, single $Fe_2B$ layer with smooth and compact morphology was observed in all samples. The comparison of Figures 4(a)–4(d) shows that the thickness of $Fe_2B$ layer increases with the exposure time boriding.

The carbides present in W2 steel reduce the boron flux into the substrate, and the interface between boride layer and substrate takes smooth morphology; this morphology is a characteristic feature for boride layers in high-alloyed steel [7, 10, 14]. Therefore, the borided layers depend on the concentration of alloying elements of the substrate, the temperature, and time exposure.

The average thickness values of $Fe_2B$ layers were calculated using the equation as set in Figure 3. In this way, Figure 5 shows the influence of the boriding time and temperature of the depth of $Fe_2B$ layers and represents a parabolic relation between the thickness of the $Fe_2B$ layer and boriding time. The average value of the largest $Fe_2B$ layer formed is about $45.86 \pm 4.13$ .6 at condition at 1273 K for 8 h and the average value of the smallest $Fe_2B$ layer formed is about $9.96 \pm 2.61$ $\mu$m at condition at 1123 K for 2 h. The $Fe_2B$ layer thickness increased with treatment time and temperature, so the growth of continuous layers of iron borides is generally recognized as a diffusion-controlled process [25].

If the adsorbed boron concentration is on the value of upper limit 59.8 mol $m^{-3}$ and lower limit $60 \times 10^3$ mol $m^{-3}$ of boron content, the iron atoms react with active boron atoms to form the $Fe_2B$ phase according to the following reaction [26]:

$$\mathrm{B\,(ads)} + 2\mathrm{Fe} \longrightarrow \mathrm{Fe_2B} \tag{10}$$

The mechanism of nucleation and growth during the boriding treatment can be described according to reports by Espinoza et al. [7] and Keddam et al. [10] during the powder pack boriding. At the beginning, there is a saturation of matrix by boron element for a time duration corresponding to $t_0^{Fe_2B}$ (time incubation), after exceeding this period of incubation, the $Fe_2B$ crystal starts nucleation on the sites energetically favorable. In addition, the growth mechanism involves three subsequence stages described by Martini et al. [4]: (i) acircular crystals of $Fe_2B$ preferentially growing on the substrate surface with their [001] axis mainly oriented parallel to the surface, (ii) several $Fe_2B$ crystals growing inside along different direction, and (iii) $Fe_2B$ crystals cause the formation of orientation [002] and growth along the direction of minimum resistance.

The EDS analysis was used to examine the element distribution of the boride layer. Figure 6 shows the SEM image and EDS line scan analysis on the cross section of the AISI W2 steels boride at 1273 K for 8 h. The EDS analysis was performed in two areas: boride layers and substrate. Figure 6(a) shows that the area of boride layer is rich in iron and boron; due to the atomic radius of $B$ (=0.09 nm), the boron atoms can diffuse easily into ferrous alloys (atomic radius of 0.124 nm). The result is the formation of a single layer of $Fe_2B$, and other elements such as vanadium, chromium, and molybdenum are present. The results also show the possible dissolution of chromium in the Fe sublattice of $Fe_2B$. The elements carbon and silicon are not dissolved in $Fe_2B$; these elements tend to displace towards

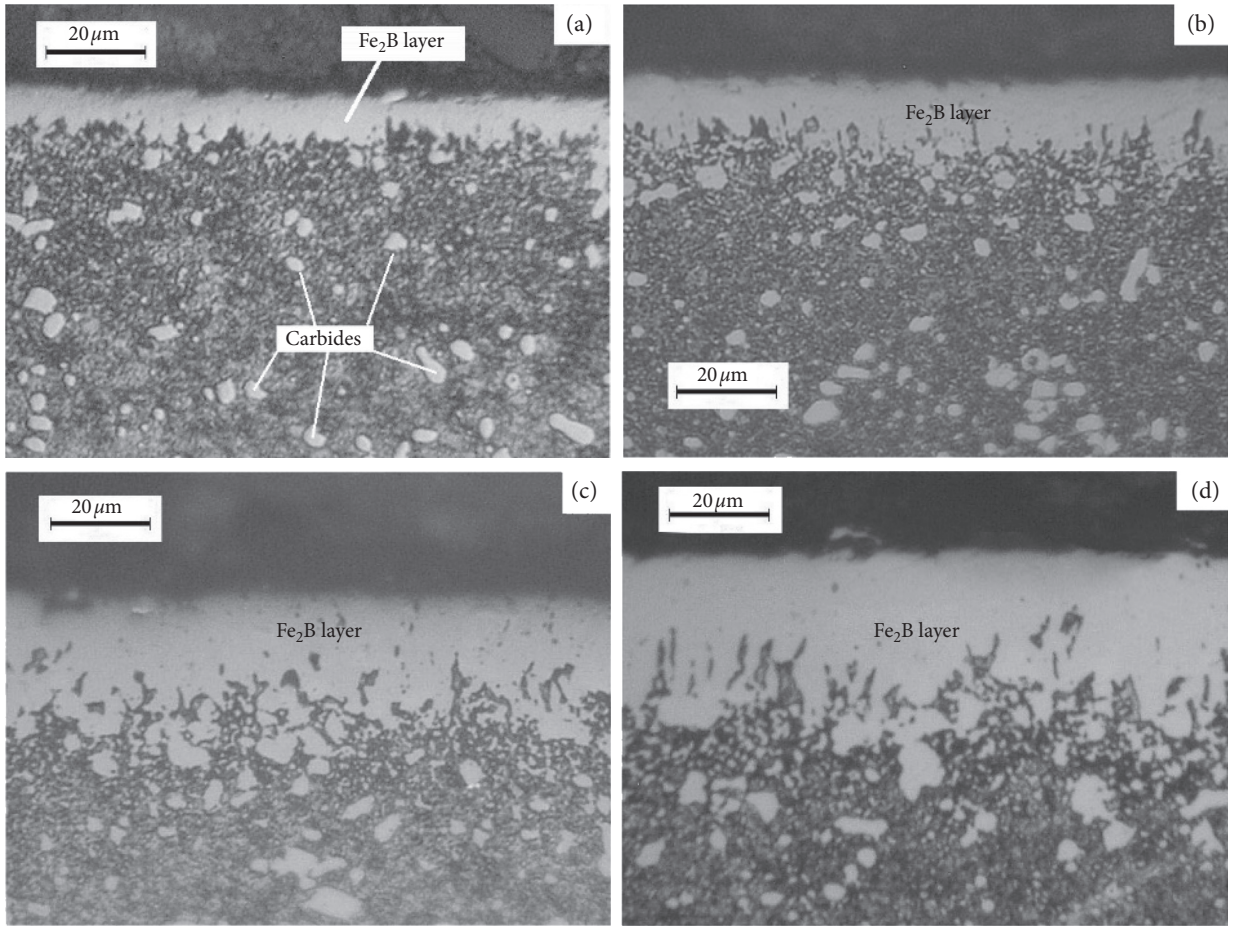


Figure 4: Cross section views of AISI W2 borided steel performed at temperature of 1173 K with (a) 2 h, (b) 4 h, (c) 6 h, and (d) 8 h of exposure.

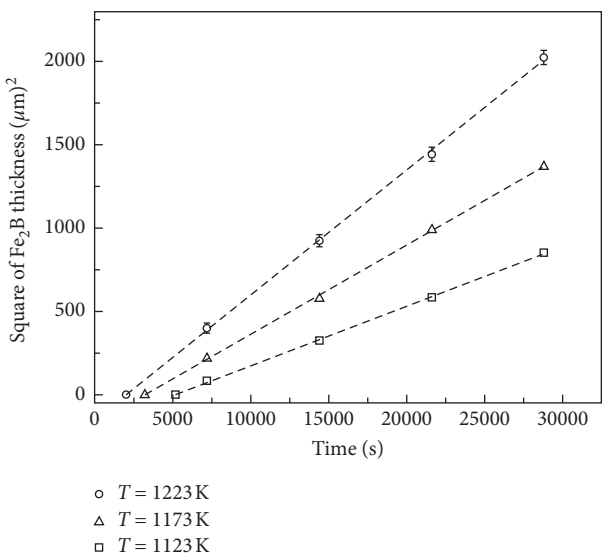


Figure 5: Growth evolution of the boride layer thickness at the surface of AISI W2 steel, $Fe_2B$ phase as a function of the exposure time.

the substrate [14, 27]. Figure 6(b) shows the area of the substrate (AISI W2) indicating the presence of the following elements: carbon, vanadium, chromium, silicon, molybdenum, and iron. In the case of vanadium, chromium, and molybdenum, spheroidal-shaped carbides are present in the AISI W2 steel matrix, and the boron is not present in the substrate.

Figure 7 shows the XRD patterns of the surface AISI W2 boride steels at a temperature of 1223 K for 8 h. The predominant phases formed in boride layers were $Fe_2B$, and the interstitial compounds such as CrB and $Cr_2B$ phases were identified. The element Cr tends to dissolve in the $Fe_2B$ phases than molybdenum. In contrast, the XRD results reported by Genel et al. [14] and Ozbek et al. [27] indicated the existence of iron boride ($FeB + Fe_2B$) for the pack boride AISI W1 and AISI W4, respectively. The formation of a single phase ($Fe_2B$) and bilayers ($FeB + Fe_2B$) in the steel substrate depends on the boron potential, and in the case of $Fe_2B$ phase formation a low boron potential is required according to reported work [4, 28].

*4.2. Growth Kinetics of $Fe_2B$ Layers.* As mentioned before, the boriding time evolution of the $Fe_2B$ thickness is shown in Figure 5. The growth rate constants $k^2$ are reflected by the slope of the straight lines in Figure 5. The intersection in the abscissa is considered as the incubation time $t_0^{Fe_2B}$. The experimental values of $k^2$ and $t_0^{Fe_2B}$ are shown in Table 1. By

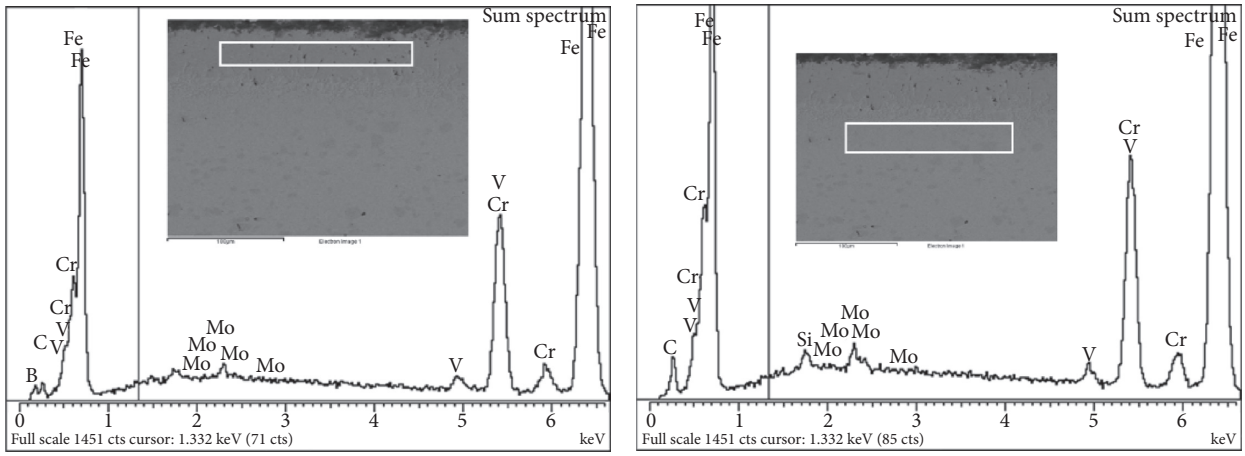


Figure 6: SEM micrograph and EDS patterns obtained in the (a) $Fe_2B$ layer and (b) substrate AISI W2.

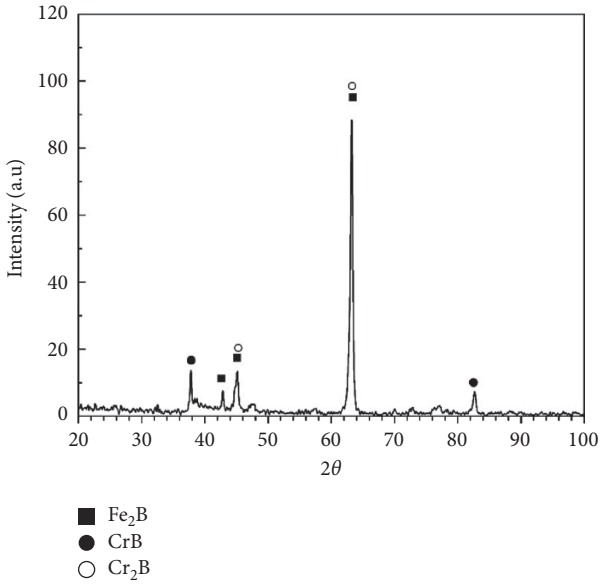


Figure 7: XRD pattern of AISI W2 boriding steel at a temperature of 1273 K with 8 h of exposure time.

Table 1: Experimental values of parabolic growth rate constants with the corresponding boride incubation time on AISI W2 by power pack boriding.

| Temperature (K)$T$ | Experimental parabolic growth constant $k^2$ ($\mu m^2$/s) | Time incubation $t_0^{Fe_2B}$ (s) |
|---|---|---|
| 1123 | 0.0749 | **4735** |
| 1223 | 0.0534 | **3205** |
| 1273 | 0.0352 | **1996** |

combining equation (8) with the experimental results demonstrated in Figure 5, the boron diffusion coefficient of boron in the $Fe_2B$ layers is estimated for each treatment time at a constant treatment temperature.

The Arrhenius equation relating the boron diffusion coefficient to the boriding temperature, with boron activation energy $Q_{Fe_2B}$ and preexponential $D_0$ factor, can be calculated from the slope and intercepts of the strapline on $Q_{Fe_2B}$ of ln $D_B^{Fe_2B}$ versus 1/T, $Q_{Fe_2B}$ as shown in Figure 8.

The boron diffusion coefficients in the $Fe_2B$ ($D_B^{Fe_2B}$) layer was expressed as a function of boriding temperature (1173 K to 1273 K) as follows:

$$D_B^{Fe_2B} = 1.07 \times 10^{-5} \exp\left(-\frac{187.696 kJ\,mol^{-1}}{RT}\right)\left(m^2 s^{-1}\right), \quad (11)$$

where $R = 8.314462$ (J/mol) is the ideal gas constant and $T$ absolute temperature (K). In this study, the calculated activation energy for the formation of the boride layer on the surface of the AISI W2 was 187.696 kJ·mol$^{-1}$; this is the necessary energy to stimulate the boron diffusion along [001] preferred direction due to the texture growth of $Fe_2B$ needles. Furthermore, the values of boron activation energy are compared with other borided tool steels found in the literature and presented in Table 2.

The activation energy for AISI W2 was attributed to the formation of $Fe_2B$, CrB, and $Cr_2B$ phases in the boride coatings; the found values of boron activation energy for AISI W2 (187.696 kJ·mol$^{-1}$) are different in comparison with borided tool steels which are attributed to the formation of phases type $(Fe)_xB$, $(Cr)_xB$, and $(Mo)_xB$. Therefore, the activation energy varies of the chemical composition of the substrate material, the boriding process, and the boron potential of the medium. In the case of boron potential, using Durborid powder mixture allows us to form a $Fe_2B$ layer on the surface; this is obtained in works of AISI O1 [7], AISI D2 [8], AISI S1 [29], and AISI W2 steels boriding by powder pack, due to lowering the boronizing potential ($B_4C$-base powder) [4].

In addition, the formation kinetics of $Fe_2B$ boride described by the diffusion model is verified by estimation of the $Fe_2B$ boride thickness as a function of the temperature and exposure time. Figure 9 shows the parameter $\beta(T)$ depends only on the temperature; this parameter has been used by several studies to estimate the thickness of the boride layers [32] and can be approximated by equation (11) using a linear fit:

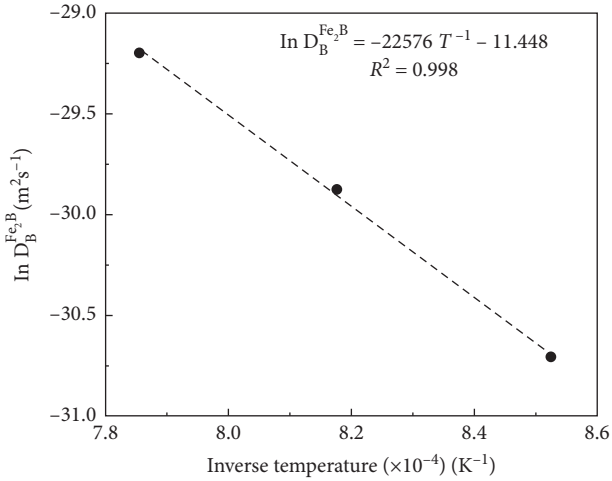


Figure 8: The behavior of the boron diffusion coefficient as a function of the boriding temperature.

Table 2: Comparison of the boron activation energy for some materials depending on the boriding method.

| Material | Boriding medium | Boriding potential | Phases in boride layer | Activation energy of Fe B kJ·mol$^{-1}$ | Activation energy of $Fe_2$ B kJ·mol$^{-1}$ | Reference |
|---|---|---|---|---|---|---|
| AISI O1 | Powder pack | Durborid powder mixture | $Fe_2B$ | — | 197.82 | Elias-Espinosa et al. [7] |
| AISI D2 | Powder pack | Durborid powder mixture | $Fe_2B$, CrB, $Cr_2B$, MoB, $Mo_4B_2$, $B_2V$ | — | 201.15 | Ortiz-Domínguez et al. [8] |
| AISI S1 | Powder pack | Powder mixture (20% $B_4C$, 10% $KBF_4$, and 70% SiC) | $Fe_2B$ | — | 199.16 | Zuno-Silva et al. [29] |
| AISI D2 | Electrochemical boriding | Molten borax ($Na_2B_4O_7$) | FeB, $Fe_2B$, CrB | 137.86 | | Sista et al. [13] |
| AISI W1 | Powder pack | Ekabor-I | FeB, $Fe_2B$ | 171.2 | | Genel et al. [14] |
| AISI H13 | Powder pack | Ekabor-I powders | FeB, $Fe_2B$, CrB, $Cr_2B$ | 186.2 | | Genel [30] |
| AISI H10 | Powder pack | Ekabor-II | FeB, $Fe_2B$, CrB, $Cr_2B$, MoB | 160.59 | | Gunes and Ozcatal [31] |
| AISI W2 | Powder pack | Durborid fresh powder mixture | $Fe_2B$, CrB, $Cr_2B$ | ------ | 187.69 | This study |

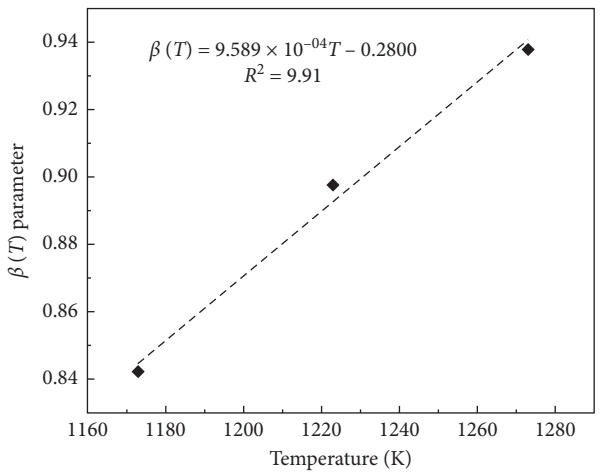


Figure 9: The evolution of $\beta$ ($T$) parameter versus the boriding temperature.

$$\beta(T) = \left(1 - \left[t_0^{Fe_2B}\frac{(T)}{t}\right]\right)^{1/2} = 9.589 \times 10^{-04}T - 0.2800. \quad (12)$$

Equation (7) can be modified as follows:

$$m = 2\beta(T)\left(\frac{C_{up}^{Fe_2B} - C_{low}^{Fe_2B}}{2C_{up}^{Fe_2B} - C_{low}^{Fe_2B}} D_B^{Fe_2B} t\right)^{1/2} \text{(m)}. \quad (13)$$

Results obtained in equation (12) are compared with experimental values. Figure 10 shows the optical images of the boride layer formed at 1259 K for 3 h and 1148 K for 1 h, and a good concordance was obtained between the experimental values of the $Fe_2B$ layer thickness and the predicted results by equation (12) as shown in Table 3. Furthermore, the thickness of $Fe_2B$ is presented in contour plots as a function of the

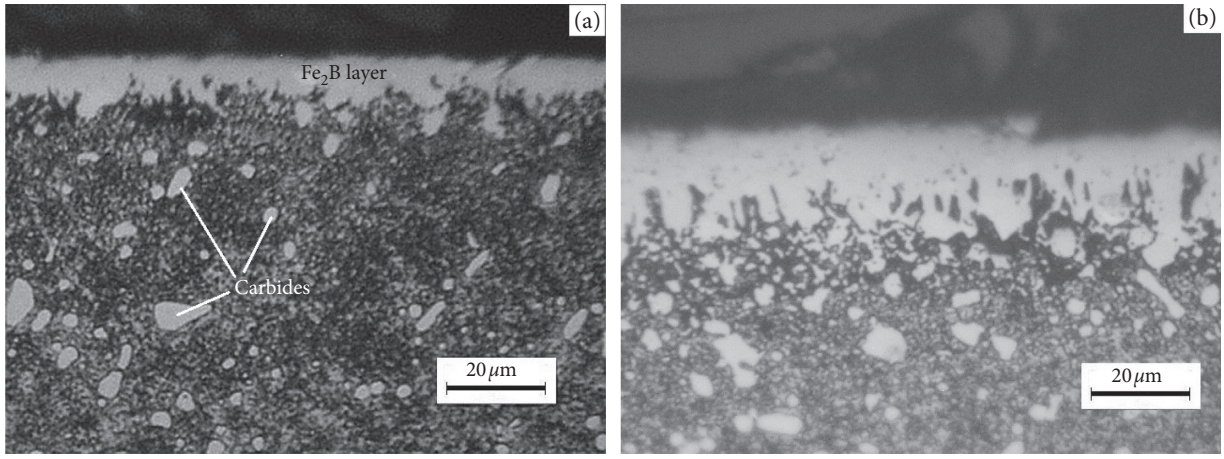


Figure 10: Cross-sectional views of AISI W2 steel borided by optical micrograph: (a) 1259 for 3 h and (b) 1148 K for 1 h.

Table 3: Prediction and estimate values of the $Fe_2B$ layer thickness.

| Temperature (K) | Time (h) | Boride layer thickness ($\mu$m) estimated by equation (10) | Experimental boride layer thickness ($\mu$m) |
|---|---|---|---|
| 1259 | 3 | 26.20 | $25.99 \pm 2$ 61 |
| 1148 | 1 | 9.25 | $9.41 \pm 1.14$ |

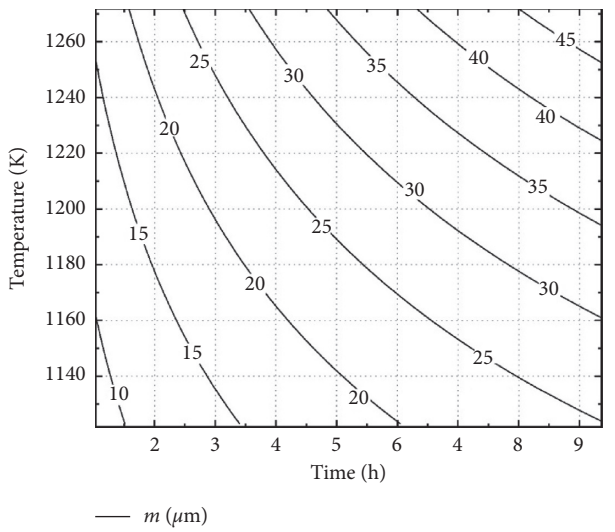


Figure 11: Contour diagram of boride layer thickness $Fe_2B$ phase of AISI W2 borided steel, as a function of temperature and time.

exposure time and temperature for powder pack boride on AISI W2. The contour diagram presented in Figure 11 can be used as a tool to select the optimal value of $Fe_2B$ layer thickness in relation to the industrial application on W2 steel. In this way, the optimal boride layer thickness on the surface of high-alloy steels ranges from 15 to 20 $\mu$m, and the $Fe_2B$ layer can be applied on tool steels for chipless forming of metals [33].

## 5. Conclusions

The Fe2B layers formed on the surface of AISI W2 steels with boron powder mixture and the growth kinetic of the boride layer were analyzed. The morphology in all the conditions was smooth and the thickness of the $Fe_2B$ layers ranged from 9.96 to 45.86 $\mu$m. The activation energy is 187.69 kJ·mol$^{-1}$, and this result was compared with the literature data on tool steel borided. In addition, a mathematical model is established to estimate the growth kinetics of $Fe_2B$ layers. This model takes the test parameters (temperature, treatment time, and incubation time) of the boriding process and the boron concentration profile in the $Fe_2B$/substrate. The effectiveness of the mathematical model is verified with both experimental measurement $Fe_2B$ layer thicknesses and mathematical model and shows a strong agreement at 1259 K for 3 h and 1148 K for 1 h conditions. Finally, contour plots can be used to select the optimum boride layer thickness for industrial applications on AISI W2 tool steels.

## Data Availability

The paper includes experimental and numerical data on AISI W2 boriding steel used to evidence the conclusions and results of this study.

## Conflicts of Interest

The authors declare that they have no conflicts of interest.

## Acknowledgments

This work was supported by PRODEP México DSA/103.5/16/10908, UPVMEX-PTC-097 and UPVMEX-PTC-095.

## References

[1] M. Kulka, *Current Trends in Boriding*, Springer International Publishing, Cham, Switzerland, 2019.
[2] J. Davis, *Surface Hardening of Steels: Understanding the Basics*, ASM International, Geauga, OH, USA, 2002.
[3] H. Okamoto, "B-Fe (boron-iron)," *Journal of Phase Equilibria & Diffusion*, vol. 25, no. 3, pp. 297-298, 2004.
[4] C. Martini, G. Palombarini, and M. Carbucicchio, "Mechanism of thermochemical growth of iron borides on iron," *Journal of Materials Science*, vol. 39, no. 3, pp. 933–937, 2004.

[5] G. J. Pérez Mendoza, M. A. Doñu Ruiz, N. López Perrusquia, and C. R. Torres San Miguel, "A microstructure obtained on AISI 1018 and AISI M2 steel by powder paste pack boriding process," *Microscopy and Microanalysis*, vol. 25, no. S2, pp. 2398-2399, 2019.

[6] M. Keddam, M. Kulka, N. Makuch, A. Pertek, and L. Małdziński, "A kinetic model for estimating the boron activation energies in the FeB and $Fe_2B$ layers during the gas-boriding of Armco iron: effect of boride incubation times," *Applied Surface Science*, vol. 298, pp. 155–163, 2014.

[7] M. Elias-Espinosa, M. Ortiz-Domínguez, M. Keddam et al., "Boriding kinetics and mechanical behaviour of AISI O1 steel," *Surface Engineering*, vol. 31, no. 8, pp. 588–597, 2015.

[8] M. Ortiz-Domínguez, M. Keddam, M. Elias-Espinosa et al., "Investigation of boriding kinetics of AISI D2 steel," *Surface Engineering*, vol. 30, no. 7, pp. 490–497, 2014.

[9] M. A. Flores-Rentería, M. Ortiz-Domínguez, M. Keddam et al., "A simple kinetic model for the growth of Fe2B layers on AISI 1026 steel during the powder-pack boriding," *High Temperature Materials and Processes*, vol. 34, no. 1, pp. 1–11, 2015.

[10] M. Keddam, M. Ortiz-Domínguez, M. Elias-Espinosa et al., "Growth kinetics of the $Fe_2B$ coating on AISI H13 steel," *Transactions of the Indian Institute of Metals*, vol. 68, no. 3, pp. 433–442, 2015.

[11] M. A. Doñu Ruiz, N. López Perrusquia, D. Sánchez Huerta et al., "Growth kinetics of boride coatings formed at the surface AISI M2 during dehydrated paste pack boriding," *Thin Solid Films*, vol. 596, pp. 147–154, 2015.

[12] M. Kulka, N. Makuch, A. Pertek, and L. Małdziński, "Simulation of the growth kinetics of boride layers formed on Fe during gas boriding in H2-BCl3 atmosphere," *Journal of Solid State Chemistry*, vol. 199, pp. 196–203, 2013.

[13] V. Sista, O. Kahvecioglu, O. L. Eryilmaz, A. Erdemir, and S. Timur, "Electrochemical boriding and characterization of AISI D2 tool steel," *Thin Solid Films*, vol. 520, no. 5, pp. 1582–1588, 2011.

[14] K. Genel, I. Ozbek, and C. Bindal, "Kinetics of boriding of AISI W1 steel," *Materials Science and Engineering: A*, vol. 347, no. 1-2, pp. 311–314, 2003.

[15] M. Elias-Espinosa, M. Ortiz-Domínguez, M. Keddam et al., "Growth kinetics of the $Fe_2B$ layers and adhesion on armco iron substrate," *Journal of Materials Engineering and Performance*, vol. 23, no. 8, pp. 2943–2952, 2014.

[16] C. M. Brakman, A. W. J. Gommers, and E. J. Mittemeijer, "Boriding of Fe and Fe-C, Fe-Cr, and Fe-Ni alloys; Boride-layer growth kinetics," *Journal of Materials Research*, vol. 4, no. 6, pp. 1354–1370, 1989.

[17] T. B. Massalski, H. Okamoto, P. R. Subramanian, and L. Kacprzak, *Binary alloy phase diagrams*, ASM International, Geauga, OH, USA, 1990.

[18] L. Yu, X. Chen, K. Khor, and G. Sundararajan, "FeB/FeB phase transformation during SPS pack-boriding: boride layer growth kinetics," *Acta Materialia*, vol. 53, no. 8, pp. 2361–2368, 2005.

[19] V. Dybkov, *Reaction Diffusion and Solid State Chemical Kinetics*, Trans Tech Publications, Switzerland, 2010.

[20] M. A. J. Somers and E. J. Mittemeijer, "Layer-growth kinetics on gaseous nitriding of pure iron: evaluation of diffusion coefficients for nitrogen in iron nitrides," *Metallurgical and Materials Transactions A*, vol. 26, no. 1, pp. 57–74, 1995.

[21] U. Roy, "Phase boundary motion and polyphase diffusion in binary metal-interstitial systems," *Acta Metallurgica*, vol. 16, no. 2, pp. 243–253, 1968.

[22] I. Campos-Silva, M. Ortiz-Domínguez, O. Bravo-Bárcenas et al., "Formation and kinetics of FeB/$Fe_2B$ layers and diffusion zone at the surface of AISI 316 borided steels," *Surf Coatings Technol*, vol. 205, no. 2, 2010.

[23] N. L. Perrusquia, M. A. Doñu Ruiz, E. Y. V. Oliva, and V. C. Suarez, "Diffusion of hard coatings on ductile cast iron," *MRS Proceedings*, vol. 1481, pp. 105–11, 2012.

[24] M. Keddam and M. Kulka, "A kinetic model for the boriding kinetics of AISI D2 steel during the diffusion annealing process," *Protection of Metals and Physical Chemistry of Surfaces*, vol. 54, no. 2, pp. 282–290, 2018.

[25] G. Palombarini and M. Carbucicchio, "Growth of boride coatings on iron," *Journal of Materials Science Letters*, vol. 6, no. 4, pp. 415-416, 1987.

[26] M. A. G. V. Boronizing, *Wemding*, Hanser Publisher, München, Germany, 1980.

[27] I. Ozbek and C. Bindal, "Mechanical properties of boronized AISI W4 steel," *Surface and Coatings Technology*, vol. 154, no. 1, pp. 14–20, 2002.

[28] E. Hernández-Sánchez, Y. M. Domínguez-Galicia, C. Orozco-Álvarez, R. Carrera-Espinoza, H. Herrera-Hernández, and J. C. Velázquez, "A study on the effect of the boron potential on the mechanical properties of the borided layers obtained by boron diffusion at the surface of AISI 316L steel," *Advances in Materials Science and Engineering*, vol. 2014, Article ID 249174, 9 pages, 2014.

[29] J. Zuno-Silva, M. Keddam, M. Ortiz-Domínguez et al., "Kinetics of formation of $Fe_2B$ layers on AISI S1 steel," *Materials Research*, vol. 21, no. 5, 2018.

[30] K. Genel, "Boriding kinetics of H13 steel," *Vacuum*, vol. 80, no. 5, pp. 451–457, 2006.

[31] I. Gunes and M. Ozcatal, "Diffusion kinetics and characterization of borided AISI H10 steel," *Materiali in Tehnologije*, vol. 49, no. 5, pp. 759–763, 2015.

[32] M. Keddam, M. Kulka, and N. Makuch, "Modeling of the growth kinetics of boride layers during the diffusion annealing process," *Physics of Metals and Metallography*, vol. 119, no. 10, pp. 927–935, 2018.

[33] W. Fichtl, "Boronizing and its practical applications," *Materials & Design*, vol. 2, no. 6, pp. 276–286, 1981.